Ensure that all changes in spelling, capitalization and other styles requested in the checklist and here in the marked pdf are made consistently throughout main text, figures and supplementary info.

Efficient Bayesian-based multi-view deconvolution

Stephan Preibisch[1,2,3], Fernando Amat[2], Evangelia Stamataki[1], Mihail Sarov[1], Robert H. Singer[2,3], Eugene Myers[1,2] and Pavel Tomancak[1]

[1]Max Planck Institute of Molecular Cell Biology and Genetics, 01307 Dresden, Germany
[2]Janelia Farm Research Campus, Howard Hughes Medical Institute, Ashburn, VA 20147, USA
[3]Department of Anatomy and Structural Biology, Gruss Lipper Biophotonics Center, Albert Einstein College of Medicine, Bronx, NY 10461, USA

Separate entities (departments or institutes) within an institution must have separate affiliations numbers.

Correspondence should be addressed to: preibischs@janelia.hhmi.org and tomancak@mpi-cbg.de

Abstract

Light sheet fluorescence microscopy is able to image large specimen with high resolution by imaging the samples from multiple angles. Multi-view deconvolution can significantly improve the resolution and contrast of the images, but its application has been limited due to the large size of the datasets. Here we present a Bayesian-based derivation of multi-view deconvolution that drastically improves the convergence time and provide a fast implementation utilizing graphics hardware.

Modern light sheet microscopes[1,2,3] are able to acquire large, developing specimens with high temporal and spatial resolution typically by imaging them from multiple directions (**Fig 1a**). The low photodamage offered by a light sheet microscope's design allows the recording of massive, time-lapse datasets that have the potential to enable the reconstruction of entire lineage trees of the developing specimen. However, accurate segmentation and tracking of nuclei and cells in these datasets remain a challenge because image quality is limited by the optical properties of the imaging system and the compromises between acquisition speed and resolution. Deconvolution utilizes knowledge about the optical system to substantially increase spatial resolution and contrast after acquisition. An advantage unique to light sheet m particular to Selective Plane Illumination Microscopy (SPIM), is the ability to o location in the specimen from multiple angles which renders the ill-po deconvolution more tractable[4-10].

Richardson-Lucy (RL) deconvolution[11,12] (**Suppl. Note ~~Chapter~~ 1, 2**) is a Bayesian-based esulting in an iterative expectation-maximization (EM) algorithm[5,13] that is often ts simplicity and performance. Multi-view deconvolution has previously been derived M framework[5,9,10], however the convergence time of the algorithm remains orders of onger than the time required to record the data. We address this problem by deriving an optimized formulation of Bayesian-based deconvolution for multiple view geometry that explicitly incorporates conditional probabilities between the views (**Fig. 1b,c**) and combine it with Ordered Subset Expectation Maximization (OSEM)[6] (**Fig. 1d)** achieving significantly faster convergence (**Fig. 1d,e,f**).

Bayesian-based deconvolution models images and point spread functions (PSFs) as probability distributions. The goal is to estimate the most probable underlying distribution (deconvolved image) that explains best all observed distributions (views) given their conditional probabilities (PSFs). We first re-derived the original Richardson-Lucy deconvolution algorithm and subsequently extended it to multiple-view geometry yielding

$$f_{RL} = \int_{x_v} \frac{\phi_v(x_v)}{\int_\xi \psi^r(\xi) P(x_v|\xi) d\xi} P(x_v|\xi) dx_v \qquad (1)$$

$$\psi^{r+1}(\xi) = \psi^r(\xi) \prod_{v \in V} f_{RL} \qquad (2)$$

Supplementary Notes 1 and 2 (no chapters)

Reserve use of "significant" for the statistical sense; quantify when used

Equations and symbols must be in an editable format, i.e., Equation Editor, MathType or the Word 2007+ equation formats

in-line expressions must have standard text formatting

where $\psi^r(\xi)$ denotes the deconvolved image at iteration r, $\phi_v(x_v)$ the input views, both as functions of their respective pixel locations ξ and x_v, while $P(x_v|\xi)$ denotes the individual PSFs (**Suppl. Note Chapter 2, 3)**. **Equation 1** denotes a classical RL update step for one view; **equation 2** illustrates the combination of all views into one update of the deconvolved image (**Suppl. Video 1**). Our equation suggests a multiplicative combination, in contrast to maximum-likelihood expectation-maximation[5] that combines RL updates by addition. We prove that **equation 2** also converges to the Maximum-Likelihood (ML) solution (**Suppl. Note Chapter 4**), while it is important to note that the ML solution is not necessarily the correct solution if disturbances like noise or misalignments are present in the input images. Importantly, previous extensions to multiple views[5,6,7,8,9,10] are based on the assumption that the individual views are independent observations (**Suppl. Fig. 2**). Assuming independence between two views implies that by observing one view, nothing can be learned about the other view. We show that this independence assumption is not required to derive **equation 2**. Thus our solution represents the first complete derivation of Richardson-Lucy multi-view deconvolution based on probability theory and Bayes' theorem.

Supplementary figures must be cited in sequential order.

As we do not need to consider views to be independent, we next asked if the conditional probabilities describing the relationship between two views can be modeled and used in order to improve convergence behavior (**Suppl. Note Chapter 7**). Assuming that a single photon is observed in the first view, the PSF of this view and Bayes' theorem can be used to assign a probability to every location in the deconvolved image having emitted this photon (**Fig. 1b**). Based on this probability distribution, the PSF of the second view directly yields the probability distribution describing where to expect a corresponding observation for the same fluorophore in the second view (**Fig. 1b**). Following this reasoning, we argue that it is possible to compute an approximate image ('virtual' view) of one view from another view provided that the PSF's of both views are known (**Fig. 1c**).

We use these 'virtual' views to perform intermediate update steps at no additional computational cost, decreasing the computational effort approximately 2-fold (**Fig. 1d and Suppl. Note Chapter 7**). The multiplicative combination (**equation 2**) directly suggests a sequential approach, where each RL update (**equation 1**) is directly applied to $\psi^r(\xi)$ (**Suppl. Fig. 2**). This sequential scheme is equivalent to the OSEM[6] algorithm and results in a 13-fold decrease in convergence time. This gain increases linearly with the number of views[6] (**Fig. 1d** and **Suppl. Fig. 4**). The new algorithm also performs well in the presence of noise and imperfect point spread functions (**Suppl. Fig. 7,8,9**). To further reduce convergence time we introduce ad-hoc simplifications (optimization I & II) for the estimation of conditional probabilities that achieve up to 40-fold improvement compared to deconvolution methods that assume view independence (**Fig. 1d,e,f, Suppl. Fig. 4, Suppl. Note Chapter 10**). If the input views show very low signal-to-noise ratio (atypical for SPIM) the speed-up is preserved but the quality of the deconvolved image is reduced. Our Bayesian-based derivation does not assume a specific noise model but it is in practice robust to Poisson noise, which is the dominating source of noise in light-sheet microscopy acquisitions (**Suppl. Fig. 6,7**). As a compromise between quality and speed we use, if not stated otherwise, the intermediate optimization I for all deconvolution experiments on real datasets.

for potential noise in the input images we added an option for Tikhonov regularization[20] (**Supplementary Fig. 7,8**). The deconvolution can be processed on the entire image at once for optimal performance or in blocks to reduce the memory requirements. The only free parameter of the method that must be chosen by the user is the number of iterations for the deconvolution process (**Supplementary Fig. 4,5**). We facilitate this choice by providing a debug mode allowing the user to inspect all intermediate iterations and identify optimal tradeoff between quality and computation time. For a typical multi-view acquisition comprising 6–8 views we suggest between 10-15 iterations.

One of the challenges in image deconvolution is to arrive at the correct solution quickly without compromising quality. We have achieved significant improvement in convergence time over existing methods by exploiting conditional probabilities between views in a multi-view deconvolution scenario, while producing visually identical or improved results at SNR's typical for light-sheet microscopy (**Fig. 2e,f** and **Suppl. Fig. 6c-h**). We have further implemented the algorithm as an open source GPU accelerated software in Fiji where it synergizes with other related plugins into an integrated solution for the processing of multi-view light sheet microscopy data of arbitrary size.

Include affiliations of researchers who provided software or materials

Acknowledgements

We thank Tobias Pietzsch for very helpful discussions, proofre[illegible] his unpublished software, Nathan Clack, Fernando Carrillo Oesterreich and Hugo Bowne-Anderson for discussions, Nicola Maghelli for two-photon imaging, Peter Verveer for his source code and helpful discussions, Michael Weber for imaging the *Drosophila* time series, Steffen Jaensch for preparing the *C. elegans* embryo, Jun Kelly Liu for the LW698 strain, Stephan Saalfeld for help with 3D rendering, P.J. Keller for supporting F.A. and the SI-SPIM dataset, Albert Cardona for access to his computer and Carl Zeiss Microimaging for providing us with the SPIM prototype. S.P. was supported by MPI-CBG, HHMI and the Human Frontier Science Program (HFSP) Postdoctoral Fellowship in R.H.S. lab, with additional support from NIH GM57071. F.A. was supported by HHMI. G.M. was supported by HHMI and MPI-CBG. P.T. was supported by The European Research Council Community's Seventh Framework Program (FP7/2007-2013) grant agreement 260746.

Author contributions

S.P. and F.A. derived the equations for multi-view deconvolution. S.P. implemented the software and performed all analysis, F.A. implemented the GPU code. E.S. generated and imaged H2Av-mRFPruby fly line. M.S. prepared and M.S. and S.P. imaged the *C. elegans* L1 sample. S.P. & P.T. conceived the idea and wrote the manuscript. R.H.S. provided support encouragement, G.M. & P.T. supervised the project.

References

Follow the format in the reference list: use *et al*. if there are more than 5 authors, and do not include issue number

1. Huisken et al. Science 13;305(5686):1007-9 (2004)
2. Keller et al. Science 322(5904):1065-9 (2008)
3. Truong et al. Nature Methods 8(9):757–760 (2011)

4. Swoger et al. Optics Express 15(13):8029-8042 (2007)
5. Shepp et al. IEEE TMI 1(2), 113-122 (1982)
6. Hudson et al. IEEE TMI 13(4), 601-609 (1994)
7. Verveer et al. Nature Methods 4(4):311-313 (2007)
8. Bonetti et al. Inverse Problems 25(1), 015002 (2009)
9. Krzic, Phd Thesis (2009)
10. Temerinac-Ott et al. IEEE TIP 21(4):1863-1873 (2012)
11. Richardson et al. JOSA 62(1):55-59 (1972)
12. Lucy et al. Astronomical Journal 79(6):745-754 (1974)
13. Dempster et al. J. Roy. Statist. Soc. Ser. B 39(1):1-38 (1977)
14. Preibisch et al. Nature Methods 7(6):418-9 (2010)
15. Long et al. Nature Methods 6(9):667-672 (2009)
16. Keller et al. Nature Methods 7(8):637-642 (2010)
17. Pitrone et al. Nature Methods 10(7), 598–599 (2013)
18. Schindelin et al. Nature Methods 9(7):676-82 (2012)
19. Pietzsch et al. Bioinformatics 28(22):3009-3011 (2012)
20. Tikhonov et al. Washington: Winston & Sons (1977)

Include the title of the thesis, the initials of the author, and the institution

Include the book title

List of Figures

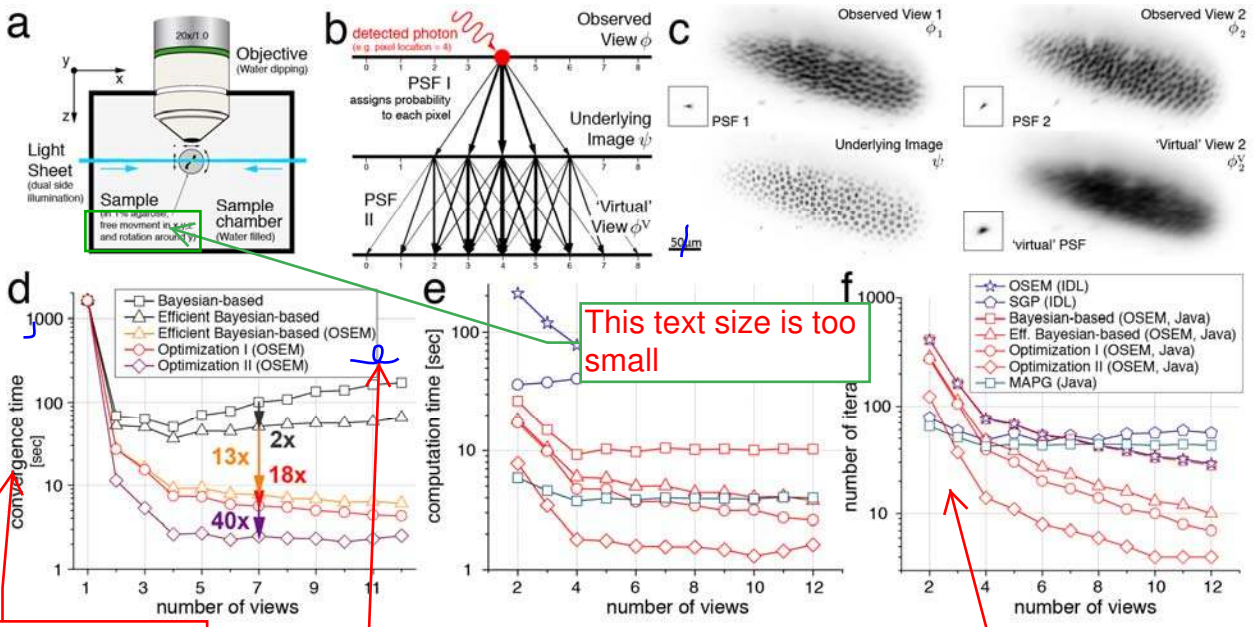

This text size is too small

Convergence time (s)

ples and performance (**a**) The basic layout of a light sheet microscope capable of multi-view acquisitions. (**b**) Illustrates the idea of 'virtual views'. A photon detected at a certain location in a view was emitted by a fluorophore in the sample; the point spread function assigns a probability to every location in the underlying image having emitted t Consecutively, the point spread function of any other view assigns to each of its own l probability to detect a photon corresponding to the same fluorophore. (**c**) Shows an example of an entire 'virtual view' computed from observed view 1 and the knowledge of PSF1 and PSF 2. (**d**) Compares the convergence time of the different Bayesian-based methods. We used a known

Remove all grid lines.

No boxes around legends

ground truth image (**Supplementary Fig. 5**) and let all variations converge until they reach precisely the same quality. Note that the increase in computation time for an increasing number of views of the combined methods (black) is due to the fact that with an increasing number of views more computational effort is required to perform one update of the deconvolved image (**Supplementary Fig. 4**) (**e**) Compares the convergence times for the same ground truth image of our Bayesian-based methods to other optimized multi-view deconvolution algorithms[5,6,7,8]. Note that part of the huge difference to OSEM and SGP is the result of not optimized IDL code. (**f**) Compares the corresponding number of iterations in comparison to other optimized multi-view deconvolution algorithms. Note that the Java and IDL implementation of OSEM perform almost identically.

Please capitalize (only) the beginning of each phrase/caption.

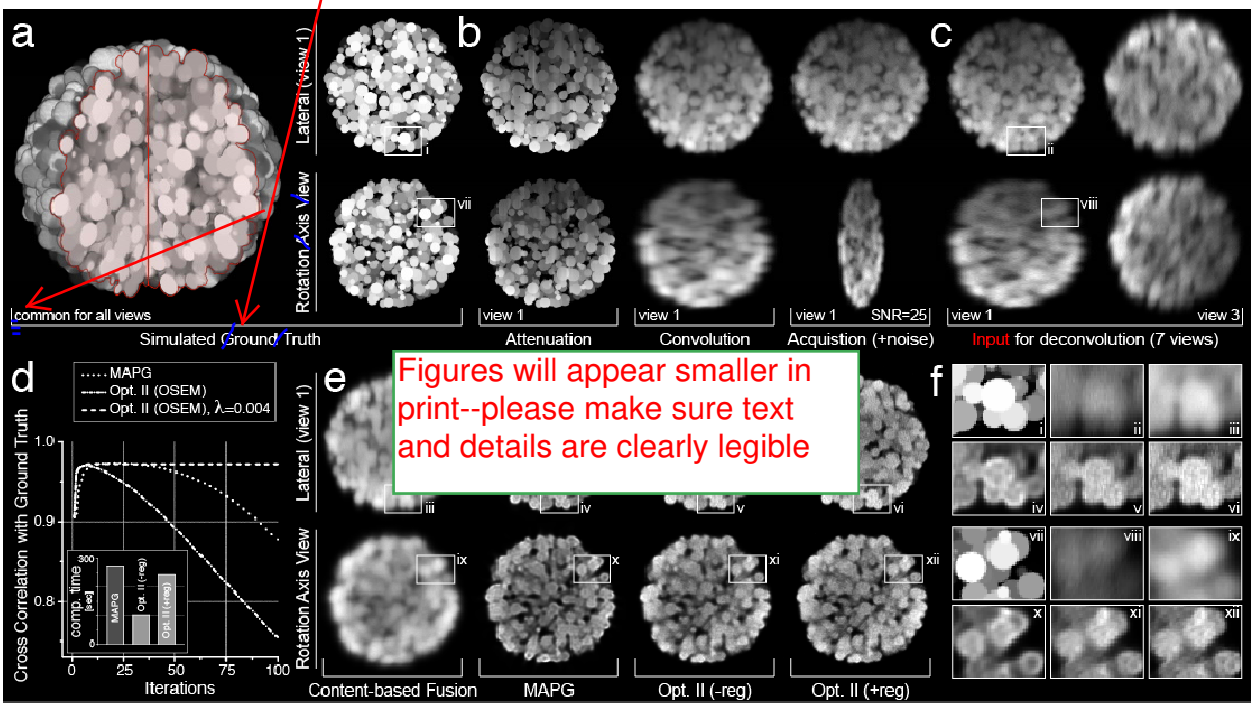

Figures will appear smaller in print--please make sure text and details are clearly legible

Separate figure panels with white space. Backgrounds should be white, not black, except for panel regions that you need to color black for contrast. Panel d should definitely not be white on black.

the generated volume in lateral direction (as seen by the SPIM camera, top) and along the rotation axis (bottom). (**b**) The same slice as in (**a**) with illumination attenuation applied (left), convolved with PSF of a SPIM microscope (middle) and image simulated using a poisson process (right). The bottom right panel shows the unscaled simulated light sheet sectioning data along the rotation axis. (**c**) Slices from view one and three of the seven views generated from (**a**) by applying processes pictured in (**b**) and rescaling to isotropic resolution. These seven volumes are the input to the fusion and deconvolution algorithms quantified in (**d**) and visualized in (**e**). (**d**) plots the cross-correlation of deconvolved and ground truth data as a function of the number of iterations for MAPG and our algorithm with and without regularization. The inset compares the computational time (both algorithms were implemented in Java to support partially overlapping datasets, **Suppl. Fig. 17**). (**e**) slices equivalent to (**c**) after content based fusion (first column), MAPG deconvolution (second column), our approach without regularization (third

column) and with regularization (fourth column, lambda=0.004). (**f**) shows areas marked by boxes in (**b,c,e**) at higher magnification.

Remove box borders around all figures and legends.

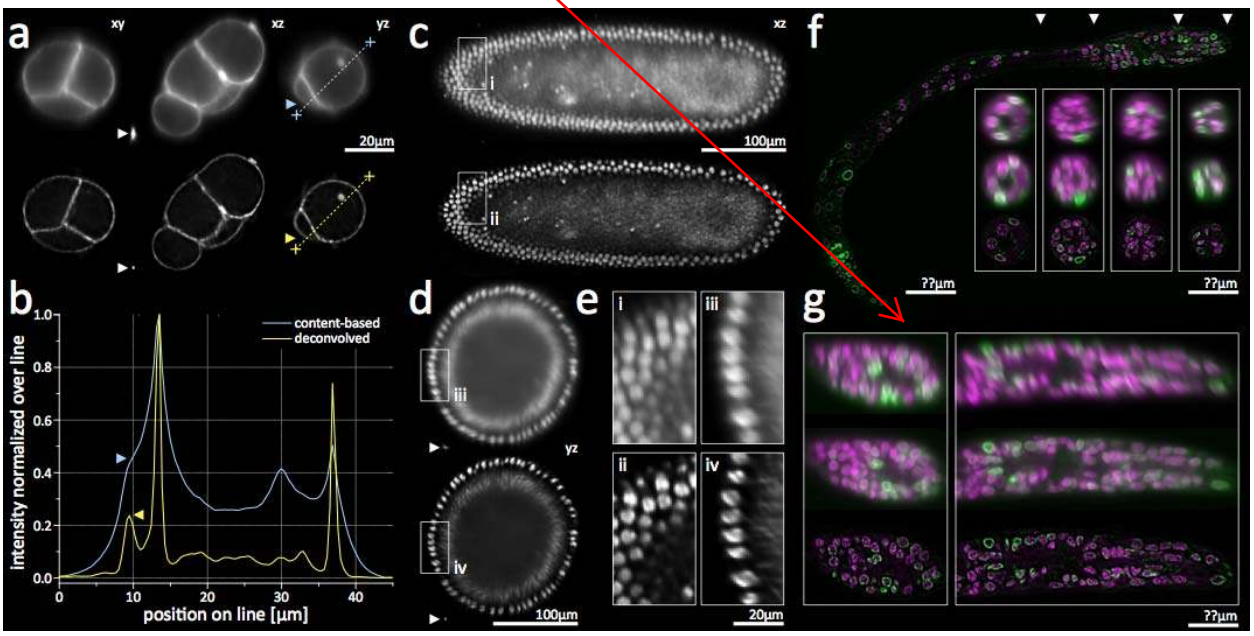

Figure 2 *Application to biological data* (**a**) Comparison of reconstruction results using content-based fusion (upper row) and multi-view deconvolution (lower row) on a 4-cell stage *C. elegans* embryo expressing PH-domain-GFP fusion marking the membranes. Dotted lines mark plots shown in (b), white arrows mark PSFs of a fluorescent bead before and after deconvolution. (**b**) Line plot through the volume along the rotation axis (yz), typically showing lowest resolution in light sheet acquisitions. Contrast along the line is locally normalized. Signal-to-noise is significantly enhanced, arrows mark points that illustrate increased resolution. (**c,d**) show cut planes through a blastoderm stage *Drosophila* embryo expressing His-YFP in all cells. White boxes mark areas magnified in (e). Detailed comparison of computation times for this dataset is shown in **Fig 1e**. (**e**) Magnified view on small parts of the *Drosophila* embryo. Left panel shows one of the directly acquired views, right panel shows a view along the rotation axis usually characterized by the lowest resolution. (**f,g**) Comparison of the deconvolved image data to the input data of a fixed *C. elegans* larvae in L1 stage expressing LMN-1-GFP (green) and stained with Hoechst (magenta). (**f**) Single slice through the deconvolved dataset, arrows mark 4 locations of transversal cuts shown below. The cuts compare two orthogonal input views (0, 90 degrees) with the deconvolved data. Note that no input view offers high resolution in this orientation approximately along the rotation axis. (**g**) The first row of the left box shows a random slice of a view in axial orientation marking the worst possible resolution of the microscope. The second row shows an input view in lateral orientation, i.e. the best possible resolution achieved by the microscope. The third row shows the corresponding deconvolved image. The box on the right shows a random slice through the nervous system. Note that the alignment of the *C. elegans* L1 dataset was refined using nuclear positions as described in **Supp. Note Chapter 15**.

You must include an Online Methods section. Please see the checklist.